ARCHIVES OF TRANSPORT *ISSN (print): 0866-9546*
Volume 76, Issue 4, 2025 ***e-ISSN (online):*** *2300-8830*
DOI: *10.61089/aot2025.a4bewn26*

SIMULATION RECONSTRUCTION OF THE PILOT EJECTION PROCESS USING THE K-36DM EJECTION SEAT

Grzegorz KOWALECZKO[1], Mariusz PIETRASZEK[2], Andrzej DŁUGOŁĘCKI[3], Mariusz IZDEBSKI[4], Stanisław OSZCZAK[5]

[1] *Department of Airframe and Engine, Faculty of Aviation, Polish Air Force University, Dęblin, Poland*

[2, 3] *Department of Air Armament, Air Force Institute of Technology, Warsaw, Poland*

[4] *Air Transport Department, Institute of Logistics and Transport, Polish Air Force University, Dęblin, Poland*

[5] *Geoinformatics and Meteorology Department, Institute of Navigation, Polish Air Force University, Dęblin, Poland*

Abstract:

The article discusses the method of reconstructing the ejection process. Measurement data were obtained during field tests on an actual object. These data served as the basis for validating the mathematical model of the seat-pilot system's motion. This model describes the spatial motion of the K-36DM ejection seat. The article includes a description of the mathematical model and a comparison of the measured motion parameters with the calculation results. It also presents computed parameters that were not recorded during the tests. Particular attention was paid to the reconstruction of the flight trajectory and seat rotation and the determination of the G-forces acting on the pilot. The primary objective of the research was to develop a mathematical model of the pilot ejection process using the K-36DM ejection seat. In addition to classical equations of motion, such as linear motion of the seat along the guide rails and motion of the seat along the rails with rotation around the lower pair of rollers, the model also considered the free motion of the seat-autopilot system, taking into account the forces acting on the seat-autopilot system. In this work, four phases of the chair movement were modeled, i.e. phase 1: After activation of the first pyrotechnic charge, the seat moves in a straight line along the guide rails until the two upper pairs of rollers disengage from the rails; phase 2: The seat continues moving along the guide rails using the lower pair of rollers until it exits the cockpit. Simultaneously, the seat begins to rotate relative to this pair of rollers; phase 3: The seat moves through the air; initially, it is propelled by the second pyrotechnic charge, providing the necessary flight altitude; phase 4: The pilot separates from the seat and descends under a parachute.

Keywords: *ejection seat, emergency system, mathematical model of ejection seat motion, simulations*

To cite this article:

Kowaleczko, G., Pietraszek, M., Długołęcki, A., Izdebski, M., Oszczak, S. (2025). Simulation reconstruction of the pilot ejection process using the K-36DM ejection seat. Archives of Transport, 76(4), 7-28. https://doi.org/10.61089/aot2025.a4bewn26

Contact:
1) g.kowaleczko@law.mil.pl [https://orcid.org/0000-0002-4376-0531]; 2) mariusz.pietraszek@itwl.pl [https://orcid.org/0000-0001-6456-4778]; 3) andrzej.dlugolecki@itwl.pl [https://orcid.org/0000-0002-4357-4341]; 4) m.izdebski@law.mil.pl [https://orcid.org/0000-0002-9157-7870]; 5) s.oszczak@law.mil.pl [https://orcid.org/0000-0003-4954-5581] – corresponding author

1. Introduction

The primary function of the ejection seat is to ensure the pilot's safe escape from the aircraft in emergency situations. The first ejection seats were developed during World War II. However, they did not guarantee complete safety - at high flight speeds, the pilot could collide with the aircraft's tail section. Additionally, it should be noted that ejection is a process often initiated during non-steady flight conditions - under both positive and negative accelerations. This means that at the initial moment, the seat is subjected to accelerations that affect its motion and thus the possibility of collision with the aircraft fuselage. Advances in seat design have eliminated this hazard. This is confirmed by documented cases of ejection seat use, for example during emergency escapes at airshows. Modern ejection seats provide full automation of the ejection process. The pilot's role is limited to initiating the process. Ejection is possible from ground level at zero aircraft speed. This capability is provided by so-called 0-0 class seats.

In aviation engineering, simulation studies are an integral support tool both at the design stage and during aircraft operation. This also applies to ejection seats. Simulating their motion requires appropriate mathematical models. These models may vary in their level of simplification. In the analyses presented here, a simplified 3-DOF planar motion model in the vertical plane (Głowiński et al., 2010; Głowiński et al., 2013) was not used. Instead, a 6-DOF model was employed, which describes the spatial (translational and rotational) motion of a rigid body (Maryniak et al., 2004).

The motion of the seat during ejection can be divided into four stages. The first two result from the seat's design, which is equipped with three pairs of rollers moving along guide rails:

1. After activation of the first pyrotechnic charge, the seat moves in a straight line along the guide rails until the two upper pairs of rollers disengage from the rails.
2. The seat continues moving along the guide rails using the lower pair of rollers until it exits the cockpit. Simultaneously, the seat begins to rotate relative to this pair of rollers.
3. The seat moves through the air; initially, it is propelled by the second pyrotechnic charge, providing the necessary flight altitude.
4. The pilot separates from the seat and descends under a parachute.

Throughout all stages of ejection, the seat-pilot system is subjected to external forces - gravity and aerodynamic force. In specific time intervals, forces generated by the pyrotechnic charges also act on the system. The first two stages can be described as the constrained motion of a rigid body. Stages III and IV represent the free motion of a rigid body. Stages I and II are crucial because the motion parameters achieved at the end of stage II have a direct impact on the free motion, including the achieved altitude, speed, and trajectory of the system. Therefore, the mathematical description of the motion was divided, with stages I and II analyzed separately and stages III and IV analyzed together.

The primary objective of the research was to develop a mathematical model of the pilot ejection process using the K-36DM ejection seat. In addition to classical equations of motion, such as linear motion of the seat along the guide rails and motion of the seat along the rails with rotation around the lower pair of rollers, the model also considered the free motion of the seat-autopilot system, taking into account the forces acting on the seat-autopilot system.

The work has been divided into four chapters. The first chapter introduces the subject of pilot ejection using ejection seats. The second chapter presents a review of the literature concerning the ejection process itself. In the third chapter, a model of the linear motion of the seat along the guides, a model of the seat's motion along the rails with rotation around the lower pair of rollers, and an analysis of experimental data are provided. A summary of the research results is presented in the fourth chapter.

2. Literature analysis

The pilot ejection process is widely discussed in the literature. The ejection process is one of the key processes occurring in aircraft, directly affecting pilot safety. Proper modeling of the strategy for managing this process (Wachnik et al., 2021; Jacyna-Gołda et al., 2015) is essential to minimize the risk of fatal accidents in aviation.

In study (Ramm et al., 1994), equations modeling this process are presented, and the optimal parameters for safe ejection are described. The ejection process is closely related to the topic of crew safety in aircraft. In study (Stępień et al., 2017), the au-

thors focused on the ejection seat as a crucial aircraft component affecting safety during military operations. Study (Yu et al., 2010) presents a numerical simulation method used to evaluate and analyze the effectiveness of aircraft egress using ejection seats in difficult situations. The ejection process was divided into four stages, for which appropriate mathematical models were developed. In the free-flight phase, quaternions were used instead of classical Euler equations describing angular velocities. The resulting equations were solved using fourth-order Runge–Kutta methods. The obtained simulation results showed good agreement with experimental data.

Artificial intelligence algorithms are often used in the context of safety in various branches of transportation, such as road, rail, and air transport (Semenov et al., 2025; Izdebski et al., 2024; et al., 2024), and have also found application in pilot ejection systems. In studies (Mao et al.,2022; Mao et al., 2011), neural networks were used to select optimal ejection parameters in cases of low-altitude ejection.

In study (Chen et al., 2007), a method for examining the aerodynamic performance of an ejection seat was proposed. The motion trajectories of the seat are derived based on its aerodynamic characteristics. An analysis of the forces acting on the ejection seat using fluid mechanics is presented in study (Rahman et al., 2023). Three-dimensional Reynolds-averaged Navier–Stokes equations were solved to obtain the aerodynamic coefficients of the ejection-seat system..

In study (Zhang, 2022), an aerodynamic analysis of an ejection-seat system at various angles of attack was carried out using numerical methods. A DES model based on the one-equation Spalart–Allmaras (S-A) turbulence model was adopted. Parallel computations were performed using the domain decomposition method, and a multiblock partition was obtained with the METIS system. Experimental data were used to validate this method.

In study (Kowaleczko et al., 2018), the authors presented a mathematical model of the pilot ejection process, taking into account the motion of the "seat + pilot" system during the ejection phase and after the pilot separates from the seat. The proposed model includes six degrees of freedom (6DOF), which makes it possible to simulate motion in space (not only along a single axis). For model verification, data specific to the K-36DM ejection seat were used, supplemented with information from other ejection seats in order to create a reliable model. In study (Głowiński et al., 2011), the authors described a model for determining the trajectory of an ejection seat in the TS-11 "Iskra" trainer–combat aircraft. The ejection seat and its operation were characterized, and simulations were performed for various aircraft speeds.

A model of the flight trajectory of an ejection seat from a jet aircraft, taking into account parameters influencing the seat's motion—such as the initial seat velocity, ejection direction and angle, aircraft altitude, distance/height from the vertical stabilizer and canopy, as well as the mass of the pilot and the ejection seat—was presented in study (Bastug et al., 2025).

The subject of pilot ejection is extensively presented in publication (Parate, 2022). The study describes the regulations and policies implemented to ensure pilot safety in the context of new ejection-seat technologies used in military fighter aircraft.

In the work (Voleti et al., 2024), the ejection process was modeled, in which the seat–dummy system is subjected to the forces generated by the seat's ejection mechanism, aerodynamic forces, drogue parachute forces, and main parachute forces. The study simulated a 0–0 ejection scenario, meaning an escape from the aircraft at zero altitude and zero speed.

Modeling the trajectory of any moving object, including an ejection seat, is crucial from the standpoint of accident risk analysis. In the works (Lasota et al., 2025; Lasota et al., 2024), a risk assessment model for the occurrence of adverse events in the transport of oversized cargo was presented, taking into account vehicle routes. In the study (Gołda et al., 2021), the trajectories of ground support vehicles were determined in order to minimize the probability of collisions with other traffic participants.

The literature review has shown that there is a lack of a comprehensive approach to determining the trajectory of an ejection seat. Most publications focus on only one phase of the motion, namely the initial moment of ejection. In the present publication, the authors present four phases of the ejection process, which are described in Chapter 1. The study considers the ejection process during banked flight as well as a scenario in which the pilot and

the aircraft remain stationary, including an analysis of the loads acting on the pilot. In the study, simulation models were used to model the pilot ejection process, which are effective tools widely employed in the literature (Szczepański et al., 2017; Jacyna-Gołda et al., 2017; Szczepańsk et al., 2014). Simulation methods have been used in traffic modeling (Jacyna et al., 2022), in the assignment of aircraft to airports (Kowalski et al., 2021), as well as in supply chain management (Izdebski et al., 2020).

3. Mathematical model of the pilot ejection process

3.1. Linear motion of the seat along the guide rails

In the analysis of phases I and II the following coordinate systems were used to analyze the motion of the ejection seat:

- $O_g x_g z_g$ – an inertial coordinate system fixed to the ground.
- $C_0 x_{es0} z_{es0}$ – a coordinate system fixed relative to the aircraft. Point C_0 defines the position of the lower rollers on the rails before ejection. The $C_0 z_{es0}$ axis coincides with the rails.
- $C x_{es} z_{es}$ – a coordinate system attached to the seat. Point C is associated with the lower rollers. The $C x_{es}$ axis is aligned with the seat base, while the $C z_{es}$ axis is aligned with the seat back.

After the initiation of the ejection process, the seat moves along the guide rails without the possibility of rotation. Therefore, the translational motion occurs along the $C_0 z_{es0}$ axis. This motion continues until the two upper pairs of rollers disengage from the guide rails. A schematic of the forces acting on the seat-pilot system after initiation is shown in Figure 1. The velocity of the system's center of mass O_{es} is the same as at point C.

The motion is caused by the following forces: T_I – the force of the first pyrocartridge, P_N – the aerodynamic normal force, Q_z – the component of the gravitational force. The T_I force acts in time interval $t \leq t_I$. The force P_N is calculated using the following formula:

$$P_N = C_N \frac{\rho |V_{es}|^2}{2} S_{es} \tag{1}$$

where S_{es} - ejection seat reference surface (backrest surface).

The velocity V_{es} is the vector sum of the aircraft velocity V_{ap} and the seat velocity along the guide rails W_C. In the coordinate system $C_0 x_{es0} z_{es0}$ it has the following components:

$$\begin{aligned} U_0 &= V_{ap} \cos \alpha_{es0}, \\ W_0 &= -V_{ap} \sin \alpha_{es0} + W_C \end{aligned} \tag{2}$$

The initial angle of attack of the seat before ejection, α_{es0}, is equal to the sum of the aircraft's angle of attack α_{ap} and the installation angle of the seat φ_{es}:

$$\alpha_{es0} = \alpha_{ap} + \varphi_{es} \tag{3}$$

Meanwhile, the angle of attack of the seat during motion α_{es} is given by:

$$\alpha_{es} = -\arctan \frac{W_0}{U_0} \tag{4}$$

The normal force coefficient C_N depends on this angle.

The weight component of the seat-pilot system depends on the pitch angle of the seat Θ_{es0} and is given by:

$$Q_{z0} = -mg \cos \Theta_{es0} \tag{5}$$

The initial pitch angle of the seat Θ_{es0} is related to the aircraft pitch angle Θ_{ap} by the following relations:

$$\Theta_{es0} = \Theta_{ap} + \varphi_{es} \tag{6}$$

The aircraft angles α_{ap} and Θ_{ap} occurring in (3) and (6) result from the flight conditions at the moment of ejection.

The lack of rotation means that the motion of the seat in the first stage can be treated as the motion of a material point along the rails (i.e. the $C_0 z_{es0}$ axis). The equations of motion take the form:

$$\begin{aligned} m \frac{dW_C}{dt} &= T_I + P_N - Q_{z0} \\ \frac{dz_{es0}}{dt} &= W_C \end{aligned} \tag{7}$$

These equations apply if the condition is met:

$$z_{es0} < l_1 \tag{8}$$

3.2. Motion of the seat along the rails with rotation around the lower pair of rollers

After the displacement by a distance of l_1, only the lower rollers remain in contact with the rails – the bottom rollers continues to move along them. As a result, the seat gains the ability to rotate around these rollers. This is shown in Figure 2. This motion continues until the lower rollers detach from the rails. To determine the equations of motion of the seat during this stage of ejection, the Lagrange method has been used. The motion has two degrees of freedom:

z_{es0} – the distance traveled by the lower rollers (point *C*) along the rails since the start of motion,

ε – the angle of rotation of the seat around the point *C*.

The Lagrange equations describing the motion of the system are as follows:

$$\begin{aligned}&\frac{d}{dt}\left(\frac{dE_k}{dW_C}\right)-\frac{dE_k}{dz_{es0}}+\frac{dE_p}{dz_{es0}}=F\\&\frac{d}{dt}\left(\frac{dE_k}{d\omega}\right)-\frac{dE_k}{d\varepsilon}+\frac{dE_p}{d\varepsilon}=M\end{aligned}\tag{9}$$

The following quantities are defined here: $W_C=\dot{z}_{es0}$ - the translational velocity along the rails, $\omega=\dot{\varepsilon}$ - the angular velocity of rotation.

The above equations require determining the kinetic and potential energy of the system in inertial frame.

To calculate these:

– the position of the center of mass of the seat in the inertial frame $O_g x_g z_g$ is determined:

$$\begin{aligned}x_g&=x_{g\,C_0}-z_{es0}\sin\Theta_{es0}+\\&\quad+R\sin(\varepsilon+\varepsilon_0-\Theta_{es})\\z_g&=z_{g\,C_0}+z_{es0}\cos\Theta_{es0}+\\&\quad+R\cos(\varepsilon+\varepsilon_0-\Theta_{es})\end{aligned}\tag{10}$$

$x_{g\,C_0}$, $z_{g\,C_0}$ - coordinates of point C_0 resulting from the motion of the aircraft, treated as known.

– the velocity components:

$$\begin{aligned}U=\dot{x}_g&=U_{C_0}-W_C\sin\Theta_{es0}+\\&\quad+\omega R\cos(\varepsilon+\varepsilon_0-\Theta_{es0})\\W=\dot{z}_g&=W_{C_0}+W_C\cos\Theta_{es0}-\\&\quad-\omega R\sin(\varepsilon+\varepsilon_0-\Theta_{es0})\end{aligned}\tag{11}$$

U_{C_0} and W_{C_0} are the components of the velocity of point C_0. This velocity is identical to the velocity of the aircraft.

$$\begin{aligned}U_{C_0}&=V_{ap}\cos(\Theta_{ap}-\alpha_{ap}),\\W_{C_0}&=V_{ap}\sin(\Theta_{ap}-\alpha_{ap})\end{aligned}\tag{12}$$

The radius R and angle ε_0 determine the position of the center of mass of the seat and are given by:

$$\begin{aligned}R&=\sqrt{x_{mc}^2+z_{mc}^2}\\\varepsilon_0&=arctan\frac{x_{mc}}{z_{mc}}\end{aligned}\tag{13}$$

The total kinetic energy of the system includes both the kinetic energy of the mass center and the rotational energy relative to the mass center is equal to:

$$\begin{aligned}E_k&=\frac{m}{2}(U^2+W^2)+\frac{I_y}{2}\omega^2=\\&=\frac{m}{2}\left(V_{ap}^2+W_C^2\right)+\frac{I_y+mR^2}{2}\omega^2-\\&-mW_CR\omega\sin(\varepsilon+\varepsilon_0)+\\&+U_{C_0}m[R\omega\cos(\varepsilon+\varepsilon_0-\Theta_{es0})-\\&-W_C\sin\Theta_{es0}]-\\&-W_{C_0}m[R\omega\sin(\varepsilon+\varepsilon_0-\Theta_{es0})-\\&-W_C\cos\Theta_{es0}]\end{aligned}\tag{14}$$

The potential energy is equal to:

$$\begin{aligned}E_p&=mgz_g=\\&=mg\left[z_{g\,C_0}+z_{es0}\cos(\Theta+\varphi_{es})+\right.\\&\left.+R\cos(\varepsilon+\varepsilon_0-\Theta_{es0})\right]\end{aligned}\tag{15}$$

By calculating the derivatives appearing in (9), we obtain the equations of motion for the seat-pilot system when it moves along the rails on the lower pair of rollers and has the ability to rotate:

$$\begin{aligned}&\frac{dW_C}{dt}-R\sin(\varepsilon+\varepsilon_0)\frac{d\omega}{dt}+\\&+\omega^2R\cos(\varepsilon+\varepsilon_0)+g\cos\Theta_{es0}=\\&=\frac{T_I+P_N}{m}-mR\sin(\varepsilon+\varepsilon_0)\frac{dW_C}{dt}+\\&+\left(I_y+mR^2\right)\frac{d\omega}{dt}-\\&-mgR\sin(\varepsilon+\varepsilon_0-\Theta_{es0})=\\&=M-P_Ax_{mc}-P_Nz_{mc}\\&\frac{dz_{es0}}{dt}=W_C\\&\frac{d\varepsilon}{dt}=\omega\end{aligned}\tag{16}$$

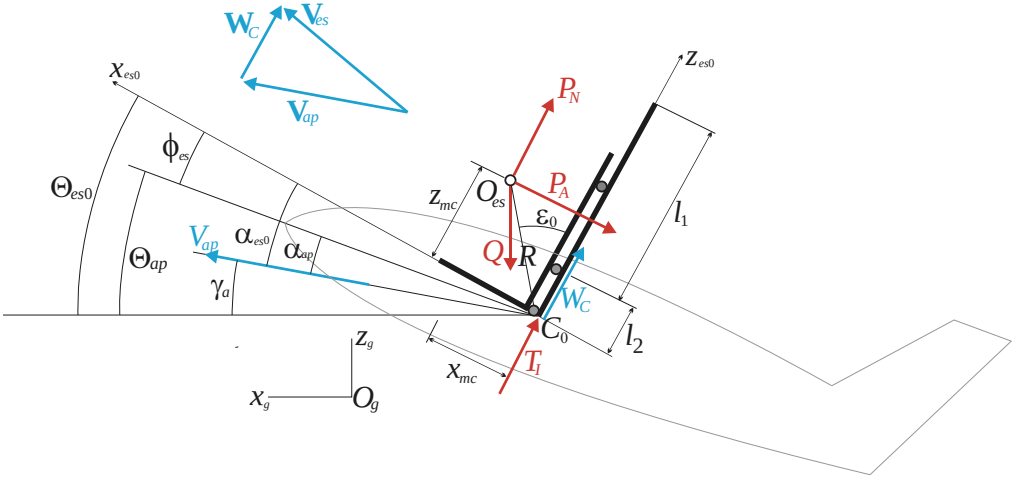

Fig.1. Diagram of forces acting during motion along the guides without rotation. Source: own work

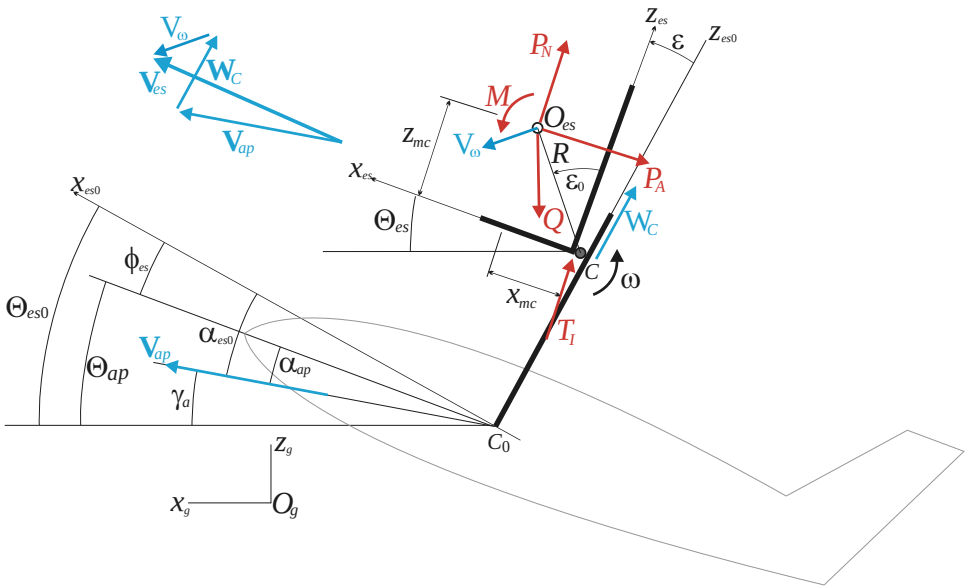

Fig.2. Diagram of forces acting during motion along the guides with rotation. Source: own work

The coefficients C_N, C_A and C_m require knowledge of the current angle of attack α_{es}. To calculate it, the components of the velocity vector of the center of mass of the seat relative to the air must be known. This vector is equal to:

$$V_{es} = V_{ap} + W_C + V_\omega \tag{19}$$

In the rotating reference frame $Cx_{es}z_{es}$ it has the following components:

$$\begin{aligned} U &= V_{ap}\cos(\alpha_{es0} - \varepsilon) - W_C \sin\varepsilon + \omega z_{mc} \\ W &= -V_{ap}\sin(\alpha_{es0} - \varepsilon) + \\ &\quad + W_C \cos\varepsilon - \omega x_{mc} \end{aligned} \tag{20}$$

The current angle of attack is calculated using a formula analogous to (4):

$$\alpha_{es} = -arctan\frac{W}{U} \tag{21}$$

3.3. Free motion of the seat-autopilot system

In the analysis of phases I and II the following coordinate systems were used to analyze the motion of the ejection seat:

- $O_g x_g y_g z_g$ – an inertial coordinate system fixed to the ground.
- $O_{es}x_{es}y_{es}z_{es}$ – a coordinate system attached to the seat. Point O_{es} is the center of mass of the seat. The $O_{es}x_{es}z_{es}$ plane is the plane of symmetry. The $O_{es}x_{es}$ axis is parallel to the seat base, and the $O_{es}z_{es}$ axis is parallel to the seat back.

The mathematical model of the free motion of the seat after losing contact with the guides results from the application of Newton's Second Law of Motion. It is similar to the models used in flight mechanics to describe the motion of flying objects. In the non-inertial reference frame associated with the seat $O_{es}x_{es}y_{es}z_{es}$, which has its origin at the center of mass O_{es}, the following equations are applied, as shown in Figure 3:

- translational motion:

$$\begin{aligned} m(\dot{U} + QW - RV) &= F_x \\ m(\dot{V} + RU - PW) &= F_y \\ m(\dot{W} + PV - QU) &= F_z \end{aligned} \tag{22}$$

U, V, W – components of the translational velocity in $O_{es}x_{es}y_{es}z_{es}$ system.

- rotational motion:

$$\begin{aligned} I_x\dot{P} - I_{xz}\dot{R} + (I_z - I_y)QR - I_{zx}PQ &= M_x \\ I_y\dot{Q} + (I_x - I_z)PR + I_{xz}(P^2 - R^2) &= M_y \\ -I_{xz}\dot{P} + I_z\dot{R} + (I_y - I_x)PQ + I_{xz}QR &= M \end{aligned} \tag{23}$$

P, Q, R – components of the angular velocity in $O_{es}x_{es}y_{es}z_{es}$ system.

- kinematic relations for angular velocities:

$$\begin{aligned} \dot{\Phi} &= P + (Q\,sin\,\Phi + R\,cos\,\Phi)\,tan\,\Theta \\ \dot{\Theta} &= Q\,cos\,\Phi - R\,sin\,\Phi \\ \dot{\Psi} &= (R\,cos\,\Phi + Q\,sin\,\Phi)/\,cos\,\Theta \end{aligned} \tag{24}$$

- kinematic relationships for linear velocities:

$$\begin{bmatrix} U_g \\ V_g \\ W_g \end{bmatrix} = \begin{bmatrix} \dot{x}_g \\ \dot{y}_g \\ \dot{z}_g \end{bmatrix} = L_{g/f} \begin{bmatrix} U \\ V \\ W \end{bmatrix} \tag{25}$$

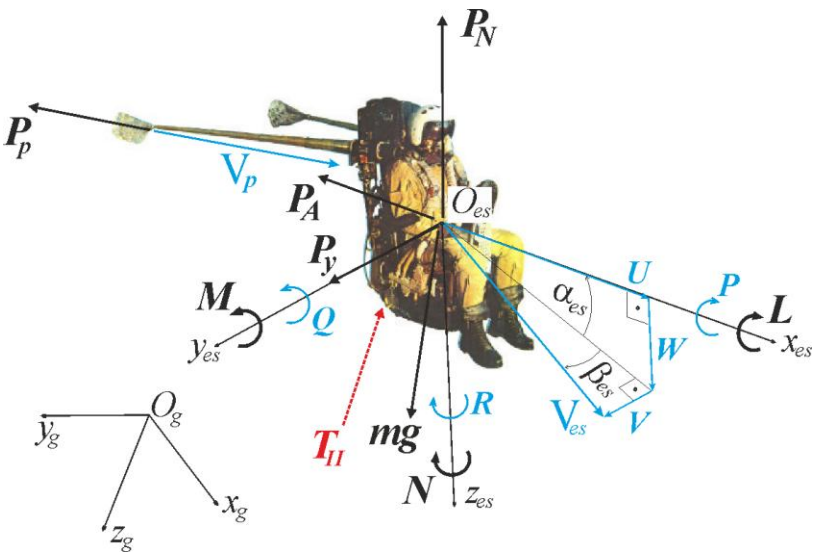

Fig.3. Coordinate systems as well as forces and moments acting on the seat-pilot system Source: Kowaleczko et al., 2018

The transformation matrix $L_{g/f} = L_{f/g}^{-1}$ is calculated by knowing the matrix:

$$L_{f/g} = \begin{bmatrix} \cos\Psi\cos\Theta & \sin\Psi\cos\Theta & -\sin\Theta \\ \cos\Psi\sin\Theta\sin\Phi - \sin\Psi\cos\Phi & \sin\Psi\sin\Theta\sin\Phi + \cos\Psi\cos\Phi & \cos\Theta\sin\Phi \\ \cos\Psi\sin\Theta\cos\Phi + \sin\Psi\sin\Phi & \sin\Psi\sin\Theta\cos\Phi - \cos\Psi\sin\Phi & \cos\Theta\cos\Phi \end{bmatrix} \quad (26)$$

Ψ, Θ, Φ – yaw, pitch and roll angles of the seat

a) Forces acting on the seat-pilot system

The resultant force F has the following components in the $O_{es}x_{es}y_{es}z_{es}$ coordinate system:

$$\begin{aligned} F_x &= Q_x - P_A + P_{px_{left}} + P_{px_{right}} + T_{IIx} \\ F_y &= Q_y + P_y + P_{py_{lef}} + P_{py_{right}} + T_{IIy} \\ F_z &= Q_z - P_N + P_{pz\_lef} + P_{pz\_right} + T_{IIz} \end{aligned} \quad (27)$$

The force components present here are:

– gravitational forces:

$$\begin{aligned} Q_x &= -mg\sin\Theta, \\ Q_y &= mg\cos\Theta\sin\Phi, \\ Q_z &= mg\cos\Theta\cos\Phi \end{aligned} \quad (28)$$

– aerodynamic forces on the seat:

$$\begin{aligned} P_A &= C_A\frac{\rho|V_{es}|^2}{2}S_{es}, \\ P_y &= C_y\frac{\rho|V_{es}|^2}{2}S_{es}, \\ P_N &= C_N\frac{\rho|V_{es}|^2}{2}S_{es} \end{aligned} \quad (29)$$

where: $|V_{es}|^2 = U^2 + V^2 + W^2$

– stabilizing parachute forces (calculations should be carried out for both parachutes – the left and the right):

The parachute is oriented perpendicular to the local airspeed V_p, generating a drag force:

$$P_p = C_{xp}\frac{\rho|V_p|^2}{2}S_p \quad (30)$$

The velocity vector V_p results from the sum of the velocity of the center of mass and the rotational motion of the seat-pilot system. Its magnitude is equal to:

$$|V_p| = \sqrt{U_p^2 + V_p^2 + W_p^2} \quad (31)$$

The individual components are calculated using the following formulas:

$$\begin{aligned} U_p &= U + Qh_{p\_z} - Rh_{p\_y}, \\ V_p &= V + Rh_{p\_x} - Ph_{p\_z}, \\ W_p &= W + Ph_{p\_y} - Qh_{p\_x} \end{aligned} \quad (32)$$

(h_{p_x}, h_{p_y}, h_{p_z}) are the coordinates of the parachute attachment point (the end of the rod).

The components of the parachute force in the $O_{es}x_{es}y_{es}z_{es}$ coordinate system are equal to:

$$\begin{aligned} P_{px} &= P_p\frac{U_p}{|V_p|}, \\ P_{py} &= P_p\frac{V_p}{|V_p|}, \\ P_{pz} &= P_S\frac{W_p}{|V_p|} \end{aligned} \quad (33)$$

The stabilizing parachute forces appear after the seat has moved along the rails by a distance l_p - the forces of the second ejection charge.

The second ejection charge moves the ejection seat beyond the area at risk of collision with the aircraft's fuselage. It operates during time $t_I \le t \le t_{II}$. Since its nozzle exit creates an angle φ_{II} with the seat backrest, the force T_{II} has the following components:

$$\begin{aligned} T_{IIx} &= T_{II}\sin\phi_{II}, \\ T_{IIy} &= 0, \\ T_{IIz} &= -T_{II}\cos\phi_{II} \end{aligned} \quad (34)$$

Based on the results of observations, it was determined that the second ejection charge does not cause the seat to rotate. This means that the angle φ_{II} is chosen in such a way that the line of action of the force $\mathbf{T}_{II}$ passes through the center of mass of the seat-pilot system.

b) Moments of forces acting on the seat-pilot system

The resultant moment M has the following components in the $O_{es}x_{es}y_{es}z_{es}$ coordinate system:

$$\begin{aligned} M_x &= L + M_{px\_left} + M_{px\_right} \\ M_y &= M + M_{py\_lef} + M_{py\_right} + M_{damp} \\ M_z &= N + M_{pz\_lef} + M_{pz\_right} \end{aligned} \tag{35}$$

There are components of moments here:

– the static aerodynamic moments of the seat

$$\begin{aligned} L &= C_l \frac{\rho|V_{es}|^2}{2} S_{es} d_{es}, \\ M &= C_m \frac{\rho|V_{es}|^2}{2} S_{es} d_{es}, \\ N &= C_n \frac{\rho|V_{es}|^2}{2} S_{es} d_{es} \end{aligned} \tag{36}$$

C_l - rolling moment coefficient, C_m - pitching moment coefficient, C_n - yawing moment coefficient, d_{es} - characteristic dimension of the seat (seat height or $d_{es} = \sqrt{4S_{es}/\pi}$).

The pitching moment coefficient has also been supplemented with a damping moment dependent on the angular velocity of pitching Q. For a flat plate, this moment is given by:

$$M_{damp} = -C_D \frac{\rho Q^2}{64} w_{es} d_{es}^4 \tag{37}$$

w_{es} - seat width, C_D - the drag coefficient of a flat plate.

– the moments from the stabilizing parachute

$$\begin{aligned} M_{px} &= P_{pz} h_{p\_y} - P_{py} h_{p\_z}, \\ M_{Sy} &= P_{px} h_{p\_z} - P_{pz} h_{p\_x}, \\ M_{pz} &= P_{py} h_{p\_x} - P_{px} h_{p\_y} \end{aligned} \tag{38}$$

The components of the aerodynamic force of the parachute are described by formulas (33).

For the chosen coordinate system, the angle of attack and the seat's slip angle, which influence the aerodynamic characteristics, are calculated using the following relationships:

$$\begin{aligned} \alpha_{es} &= -\arctan\frac{W}{U}, \\ \beta_{es} &= \arctan\frac{V}{\sqrt{U^2 + V^2 + W^2}} \end{aligned} \tag{39}$$

4. Data for calculations

4.1. Mass and geometric data

The calculations were performed for the K-36 DM ejection seat. Its geometry is shown in Figure 4 and Table 1,2. As a result of the burning of propellant charges, the mass of the seat changes. This was taken into account in the simulations by using the data collected in the table. The data were obtained from the literature and during measurements of the seat prototype.

Table 1. The mass of the ejection seat. Source: own work based on Dowództwo Wojsk Lotniczych, 1985

Masses		**Moments of inertia**	
pilot mass m_p	78 kg	I_x	33.78 kgm^2
seat mass at launch m_{es}	125 kg	I_y	38.97 kgm^2
first stage mass m_I	8 kg	I_z	13.68 kgm^2
second stage mass m_{II}	3.7 kg	I_{xz}	-8 kgm^2
headrest with parachute mass m_{hr}	18.5 kg		
rescue container mass m_{rc}	9 kg		

Table 2. The characteristics of the ejection seat. Source: own work based on Dowództwo Wojsk Lotniczych, 1985

length of the rails	l=1.045m
reference area of the seat (backrest area)	S_{es} =0.69m^2
characteristic dimension of the seat (seat height)	d_{es}=1.24m
reference area of the paraschute	S_p =0.06m^2
position of the left parachute	h_{p_x}=-2.06m h_{p_y}=-0.283m h_{p_z}=-0.55m
position of the right parachute	h_{p_x} =-2.06m h_{p_y} =0.283m h_{p_z} =-0.55m

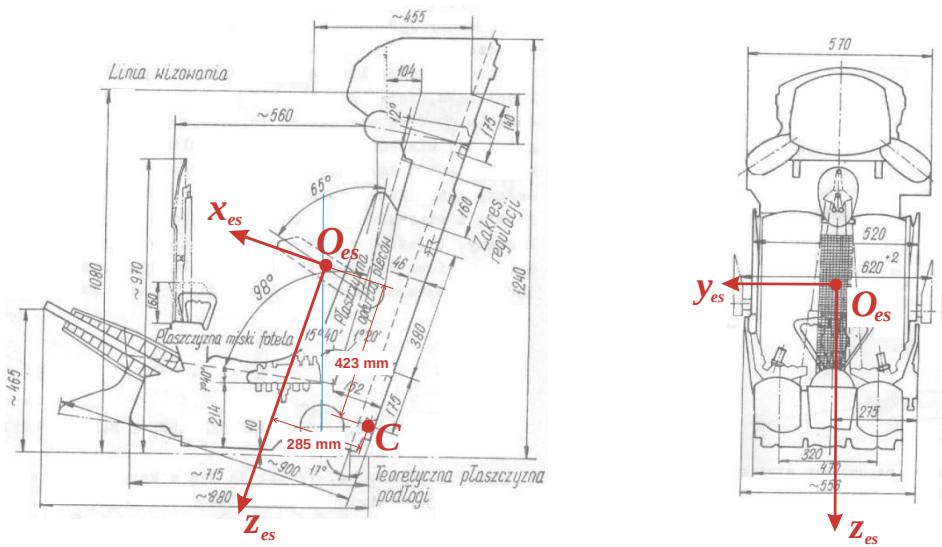

Fig. 4. Basic geometric data of the K-36DM ejection seat. Source: own work based on Dowództwo Wojsk Lotniczych, 1985

The simulations required knowledge of the aerodynamic characteristics of the seat. The aerodynamic coefficients C_A, C_N and C_m depend on the angle of attack of the seat α_{es}, while the coefficients C_y, C_l and C_n depend on the sideslip angle β_{es}.

Due to the lack of original, reliable aerodynamic characteristics of the K-36DM ejection seat, the simulations used the characteristics provided in (Szajnar et al., 2010; Szendzielorz et al., 1986), which were obtained from wind tunnel tests of the SK seat. However, these characteristics have a limited range. To estimate the coefficient values for other angles, the characteristics of another seat, provided in (Reichenau, 1972), can be considered. Figures 5-10 display the aerodynamic characteristics used in the calculations.

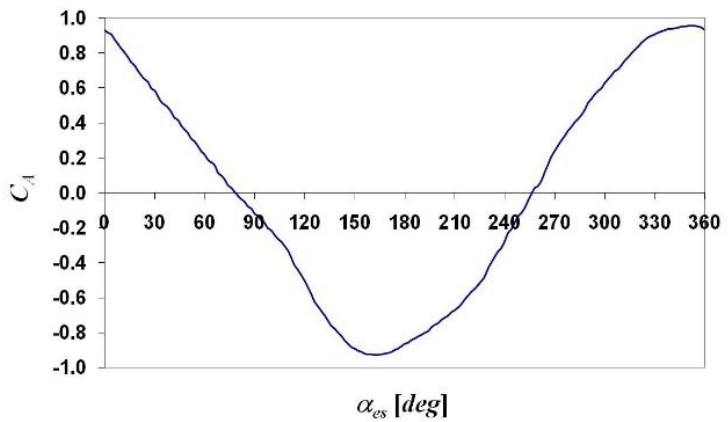

Fig. 5. Tangential force coefficient. Source: own work

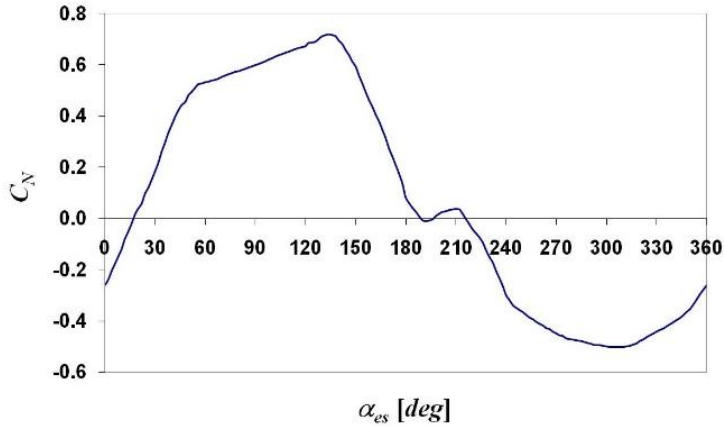

Fig. 6. Normal force coefficient. Source: own work

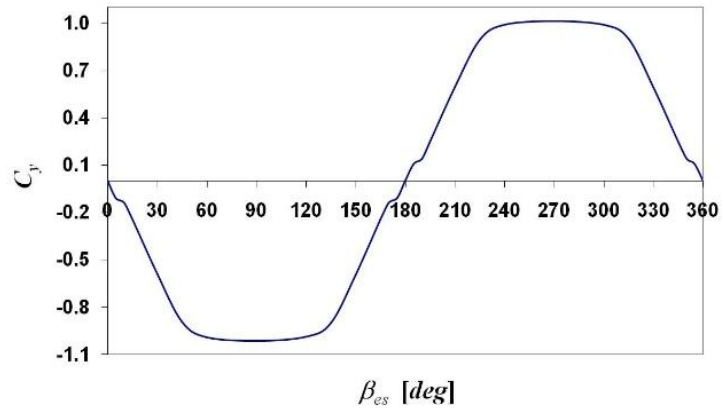

Fig. 7. Lateral force coefficient. Source: own work

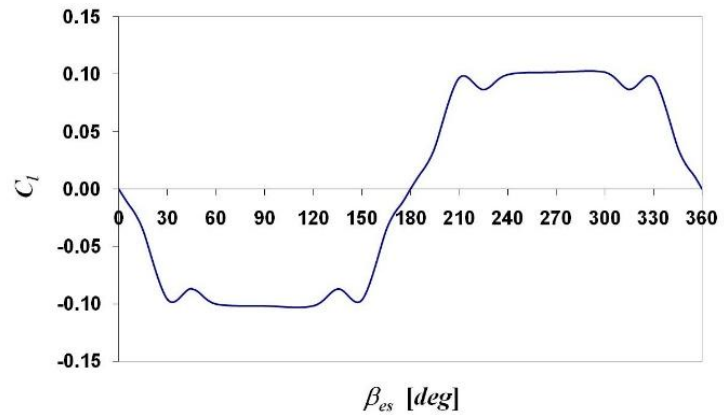

Fig. 8. Rolling moment coefficient. Source: own work

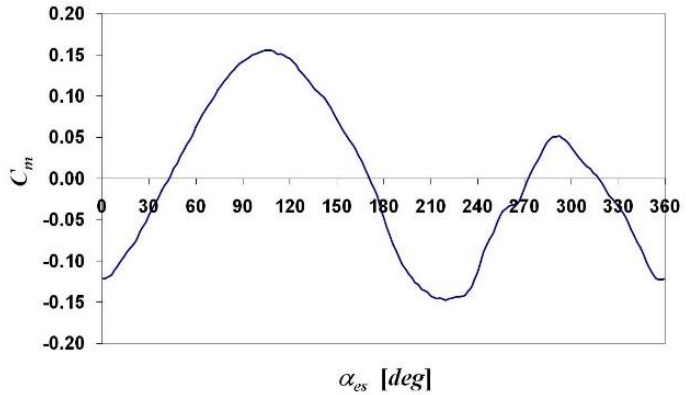

Fig. 9. Pitching moment coefficient. Source: own work

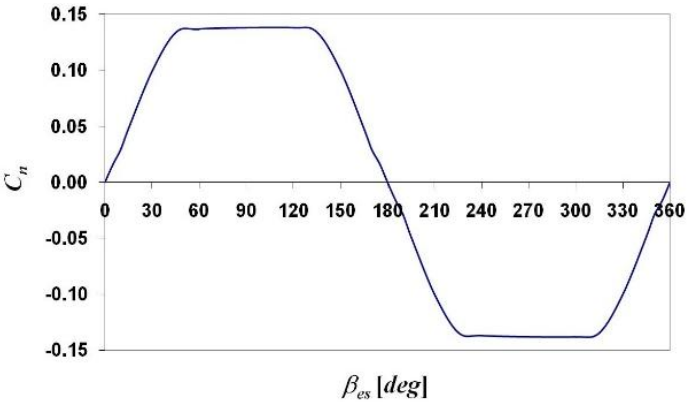

Fig. 10. Yawing moment coefficient. Source: own work

For the damping of the seat's rotational motion, a value of C_D=2 was adopted. Meanwhile, for the stabilizing parachutes controlling the seat's motion, C_{xs}=1.4 was used.

4.2. Forces of the ejection charges

In the initial phase of ejection, the seat-pilot system is subjected to the forces from two ejection charges, which operate sequentially. The magnitude of the first-stage ejection charge force T_I is unknown. However, the seat's description specifies that the first-stage ejection charge operates for approximately 0.2 seconds and should provide a minimum exit velocity of 13.6 m/s. During the calculations, it was estimated that this force is equal to T_I=27000N. This force is responsible for initiating the seat's movement and ensuring its safe exit from the aircraft's cabin. The specific magnitude and duration of this force are crucial for determining the seat's velocity and trajectory during ejection.

The second-stage charge force T_{II} is crucial for ensuring the seat's further separation from the aircraft after the first charge's work is finished, and its value directly impacts the trajectory and safety of the ejection process. The duration of the force T_{II} from the second-stage ejection charge and its magnitude can be estimated based on literature or other available data. According to (Dowództwo Wojsk Lotniczych, 1985), this force acts for 0.4 seconds after the first-stage has completed its work and should not be less than 3300 daN. However, studies conducted at the AFIT (Polish Air Force Institute of Technology) indicate that these values are debatable. Figure 11 shows the results of laboratory tests for the second-stage ejection charge.

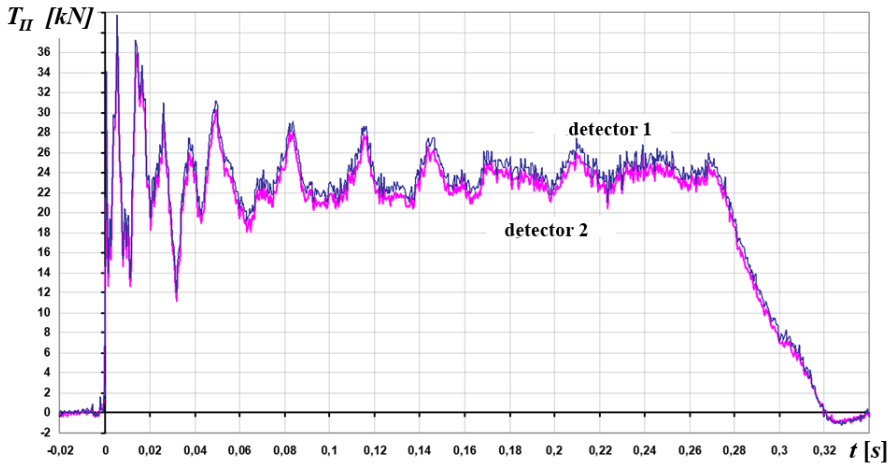

Fig. 11. Force profile of the second-stage ejection charge over time. Source: own work

4.3. Analysis of experimental data

In 2018, a series of experimental studies were conducted to identify the motion of the ejection seat. These studies were part of an investigation into the causes of an aviation accident that occurred during an emergency ejection from a MiG-29 aircraft. Special attention was given to the case of ejection from an aircraft that was stationary on the runway. For these specific conditions, a rich set of video and measurement data was available, obtained from tests carried out at a testing range. The frame-by-frame analysis of the films allowed for the identification of all stages of the ejection process, as well as the reconstruction of the seat's trajectory and rotation during the experiments.

Figure 12 shows the reconstructed trajectory of the seat-pilot system, while Figure 13 presents the change in the seat's pitch angle up to the moment of the headrest ejection. These trajectories serve as the basis for verifying the accuracy of the seat motion simulation model.

From the graph shown in Figure 13, an important conclusion can be drawn regarding the operation of the second-stage ejection charge. Analyzing this graph, it is evident that during its operation, the angular velocity of the seat-autopilot system remains constant, and the pitch angle increases linearly. This linear relationship also applies to the free rotation until the moment the headrest is ejected. This indicates that the second-stage ejection charge does not generate a pitching moment - its line of action passes through the center of mass of the system.

Therefore, the cause of the angular velocity, which leads to the rotation, should be sought in the first phase of motion when the seat exits the aircraft. This rotation occurs while the seat moves along the rails on the last — lower pair of rollers. The motion model for this phase is described in section 2.2.

a) Case 0-0

Based on the described models of ejection seat motion, a series of simulations were conducted under various initial conditions, including the 0-0 ejection scenario.

The 0-0 ejection refers to the case where both the aircraft and the pilot are at rest (i.e., the aircraft is stationary on the runway, and the pilot is seated in a stationary position within the cockpit). Simulations of this scenario are critical for understanding how the seat behaves during ejection under such specific conditions.

By running these simulations, the performance of the ejection seat can be assessed, ensuring that the seat functions correctly and safely in different real-world situations, especially during emergencies when the aircraft is not in motion.

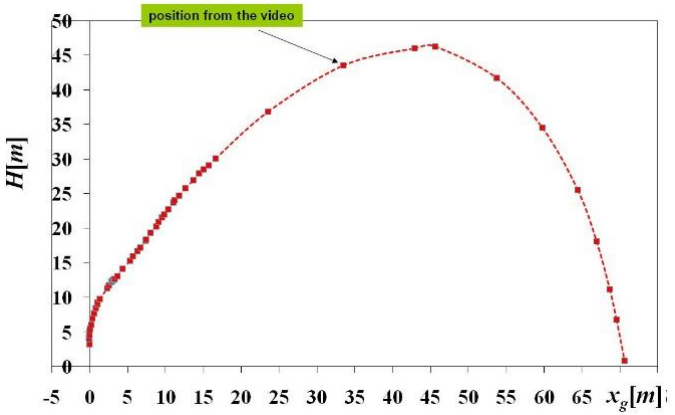

Fig. 12. Trajectory of the seat during ejection. Source: own work

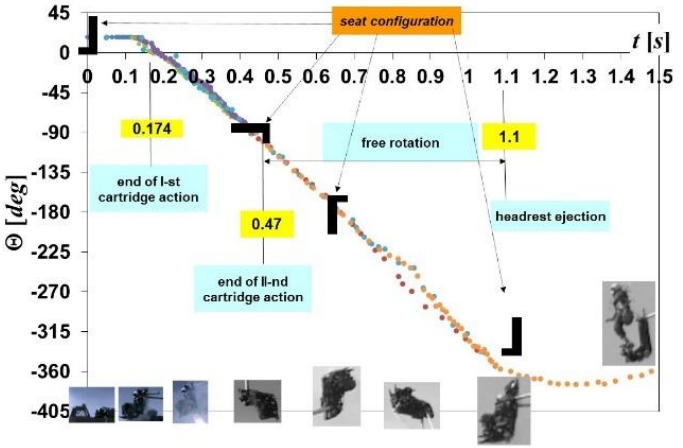

Fig. 13. Seat pitch angle during ejection. Source: own work

The Case 0-0 refers to an ejection scenario in which both the aircraft and the pilot are at rest. This is one of the most challenging ejection cases because the aircraft does not have an initial velocity that could assist in ejecting the seat from the cockpit. The 0-0 case typically applies to situations where the aircraft is stationary on the ground (e.g., on an airport runway), and the ejection is triggered due to an emergency in which the pilot needs to exit the cockpit. For these initial conditions, extensive research material obtained during field tests was available.

Figure 14 shows the trajectory obtained from the film and the trajectory calculated for the ejection case without wind, as well as with a wind speed of 3 m/s blowing in the opposite direction of the ejection. There is a strong agreement between the trajectories in the first phase of flight. In the second phase, a difference appears. This could be related to the fact that during the tests, the symmetry of the seat's motion was disrupted — the seat performed a rotation around the longitudinal axis $O_{es}x_{es}$. Figure 15 presents the trajectory, showing the position of the seat at various points along the path. The images of the seat are taken from the analyzed film.

Figure 16 shows the change in the seat's pitch angle. To facilitate the analysis of the plots, the figure was supplemented with film frames showing

the seat's positions. A very good agreement can be observed between the simulation results and the pitch angles measured from the film. Only after the headrest is jettisoned do differences appear — in reality, the seat's rotation is stopped, while in the simulations the seat continues to rotate. This rotation can be eliminated by including an additional force from the headrest's pyrotechnic charge in the equations of motion. Unfortunately, no information is available regarding the magnitude and duration of this force. Therefore, in the calculations it was experimentally adjusted to stop the rotation. The results of these calculations are shown by the black curve.

Figure 17 shows the seat's vertical velocity. It indicates that during the operation of the I-st pyrotechnic cartridge, this velocity increases linearly. After the first-stage cartridge finishes firing, the velocity reaches 18 m/s, while by the end of the second-stage cartridge operation, it reaches 30 m/s.

Figures 18 and 19 show the calculated accelerations acting on the seat along the $O_{es}x_{es}$ and $O_{es}z_{es}$ axes. During the operation of the first-stage pyrotechnic cartridge, the dominant acceleration is n_z in the head-to-feet direction, reaching nearly 13g. It increases sharply after the activation of the second-stage cartridge, reaching values of 17g. Due to the inclusion of the T_{II} force component along the $O_{es}x_{es}$ axis in the calculations, an additional acceleration n_x appears, ranging between 5 and 6g.

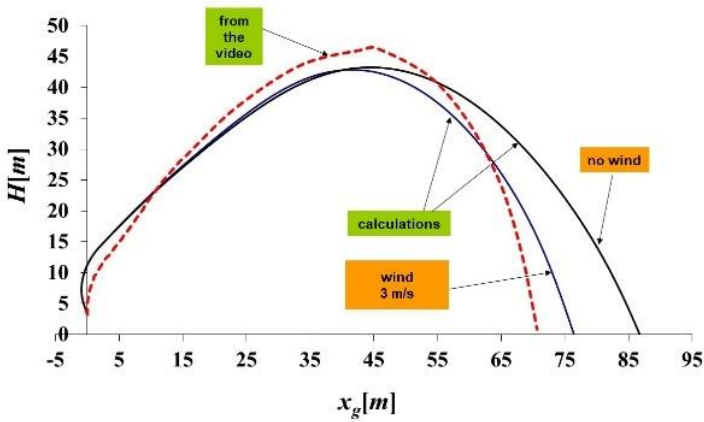

Fig. 14. Calculated and recorded flight trajectory. Source: own work

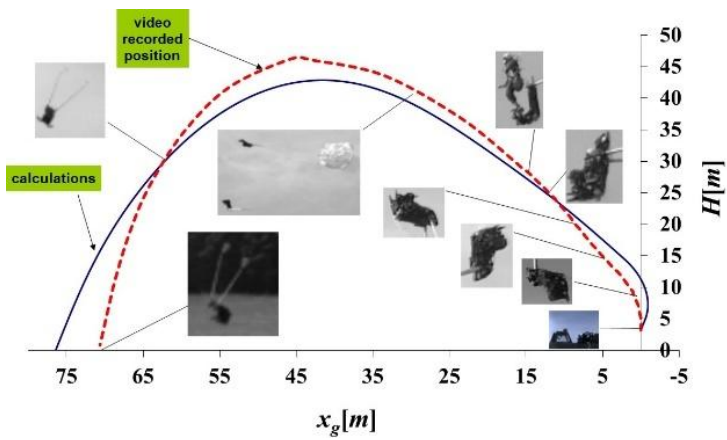

Fig. 15. Flight trajectory and seat position. Source: own work

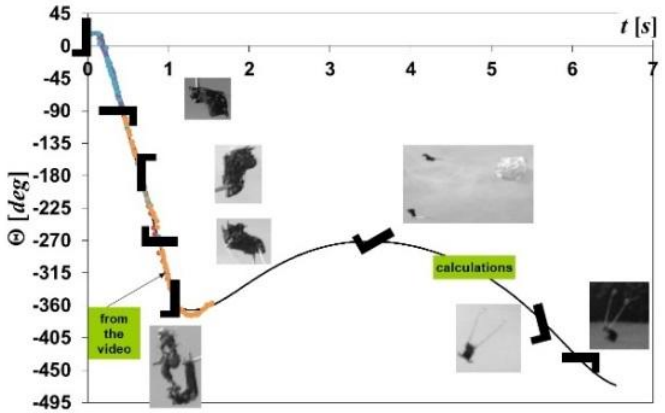

Fig. 16. Seat pitch angle until the headrest is jettisoned. Source: own work

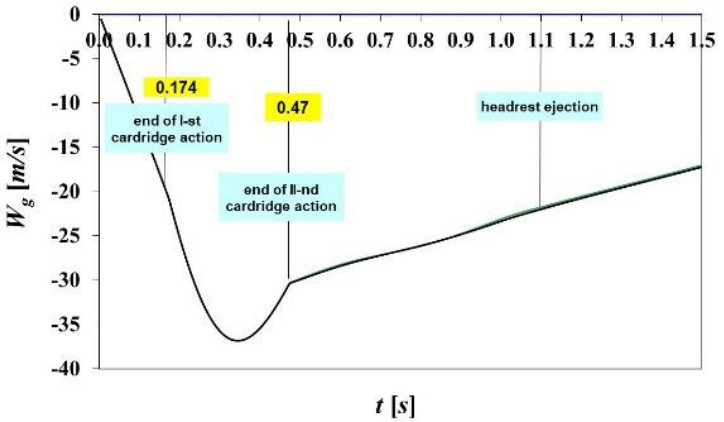

Fig. 17. Vertical velocity of the seat. Source: own work

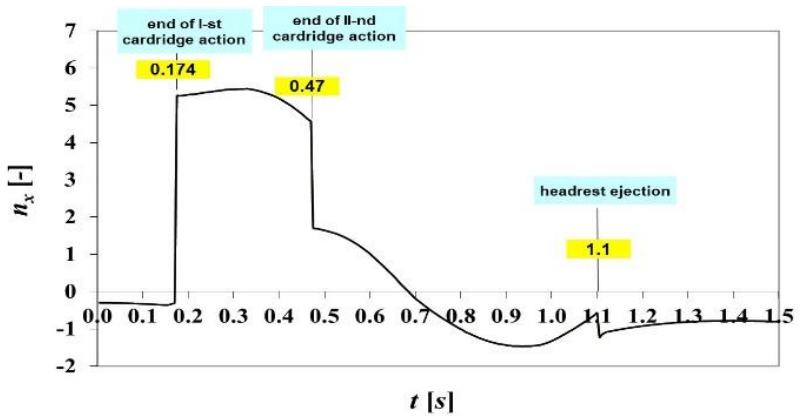

Fig. 18. G-Force along the $O_{es}x_{es}$ axis. Source: own work

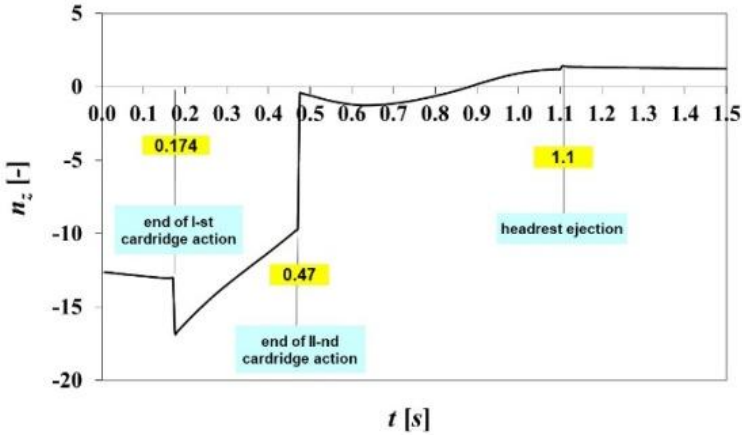

Fig. 19. G-Force along the $O_{es}z_{es}$ axis. Source: own work

The results obtained show that for the 0-0 ejection scenario, the ejection is safe – the pilot moves forward without colliding with the aircraft. The achieved maximum altitude ensures the parachute deployment. The calculated overload, although significant, do not exceed the permissible limits, which for short-duration accelerations should be in the range of 15 to 20 g.

b) Ejection in horizontal flight

It refers to the process of ejecting a pilot or crew member from an aircraft while the aircraft is flying horizontally. This type of ejection occurs when the aircraft is not in a steep climb or descent, and the ejected seat must deal with the aerodynamic conditions of level flight, including the aircraft's speed and altitude, as well as potential forces acting on the pilot during ejection.

Using the developed simulation program, ejection calculations were performed during level flight at various speeds. The flight conditions of the aircraft that affect ejection, such as the angle of attack and the aircraft's pitch angle, were calculated based on the balance of forces acting on the aircraft.

This approach allows for the determination of how these flight parameters influence the ejection process, ensuring that the pilot's safety during ejection is maintained regardless of the aircraft's speed or attitude.

Figures 20 to 23 show sample results obtained for different aircraft flight speeds: 0, 50, 100, and 200 m/s. In each case, it was assumed that the ejection height was 0 meters, and the wind from the front was blowing at a speed of 3 m/s.

From Figure 20, it is evident that the higher the flight speed, the greater the distance the seat travels -over 350 meters at a speed of 200 m/s. The maximum altitude ranges from 50 to 60 meters. The increase in flight speed reduces the maximum pitch angle of the pilot (face-down). This is shown in Figure 21, which concerns the first phase of the flight, up to the moment the pilot separates from the seat. While for the 0-0 conditions the seat rotates at a constant speed, in the case of ejection during level flight, this rotation is halted and then changes direction. This is the result of the stabilizing parachutes' effect. Figure 21 indicates that the maximum seat pitch angle ranges from -72° for V_s=50 m/s to -28° for V_s =200 m/s. These results correspond to the ejection scheme shown in (Dowództwo Wojsk Lotniczych, 1985) and presented in Figure 22.

Figure 23 shows the distance between the center of mass of the seat and the top of the vertical stabilizer. It can be seen that the increase in flight speed leads to a decrease in this distance. However, the seat does not collide with the aircraft, which continues its straight-line flight.

c) Ejection during banked flight

Simulations were also conducted to assess the effect of the aircraft's bank angle on the ejection process. It was assumed that at the moment of ejection, the aircraft is in horizontal flight at an altitude of 100 meters with a speed of 200 m/s.

Figure 24 shows the trajectory of the seat, while Figure 25 presents the distance between the seat's center of mass and the tip of the vertical stabilizer. An increase in altitude can only be observed at bank angles less than 90°. The smallest distance between the seat and the stabilizer occurs during ejection without any bank angle. This distance is reached at approximately 0.3 seconds and amounts to 2.8 meters. The results also show that the seat's trajectory curves to the right, with the greatest deviation from the initial flight path being 95 meters, achieved at a bank angle of 90°.

5. Conclusions

The developed seat–pilot system motion model enables the simulation of ejection under various flight conditions. The simulations provide a representation of the spatial motion. The reliability of the results was verified to a limited extent by comparing them with experimental data. A broader scope of validation would be possible after obtaining the aerodynamic characteristics of the K-36 DM seat. This is particularly important since this seat is certified for use over a wide range of speeds - accounting for air compressibility may be necessary. Currently, the model allows for determining accelerations only at the center of mass. It is desirable to determine the accelerations acting on different parts of the pilot's body, such as the head. This would require expanding the model to include a representation of the human body.

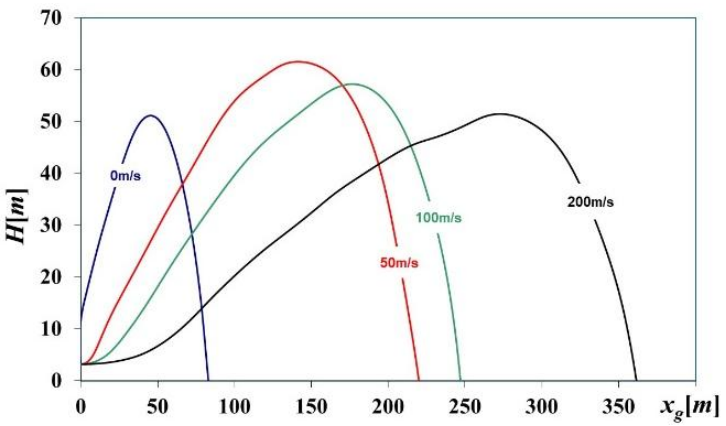

Fig. 20. Seat flight trajectory. Source: own work

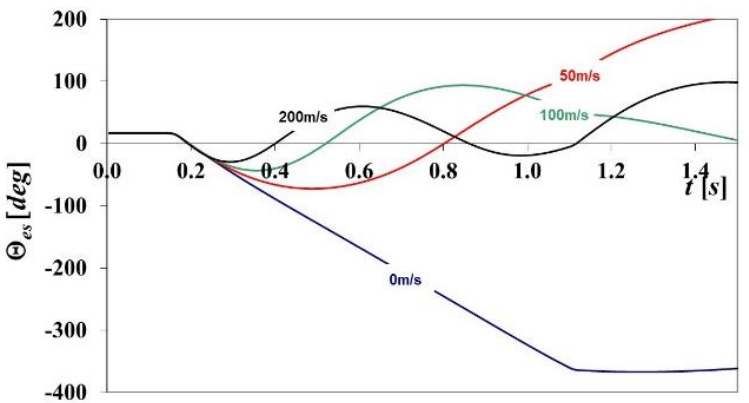

Fig. 21. Seat pitch angle. Source: own work

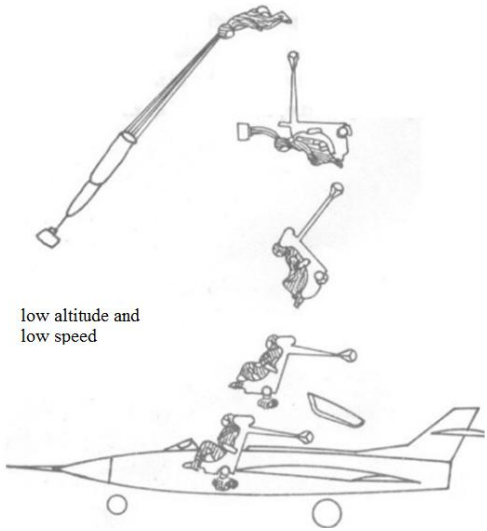

Fig. 22. Ejection schematic. Source: own work based on Dowództwo Wojsk Lotniczych, 1985

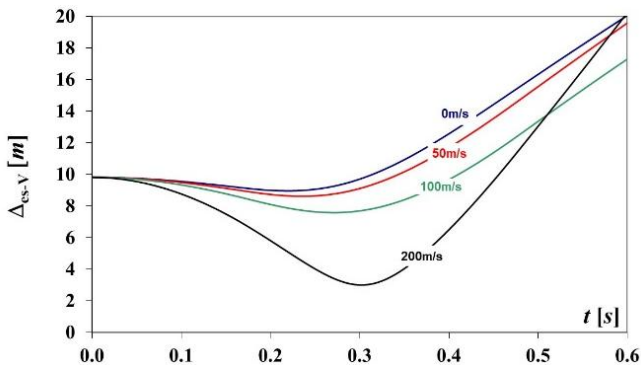

Fig. 23. Distance between the seat and the vertical stabilizer. Source: own work

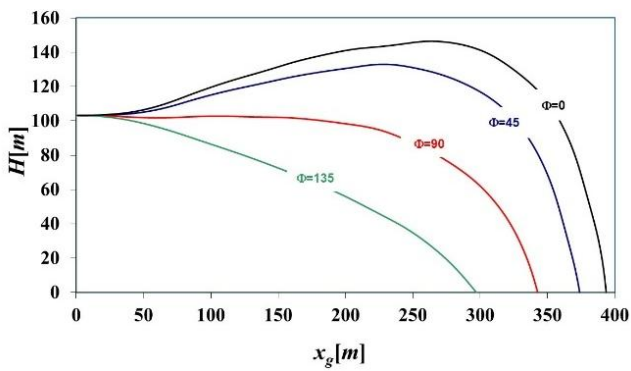

Fig. 24. Seat flight trajectory. Source: own work

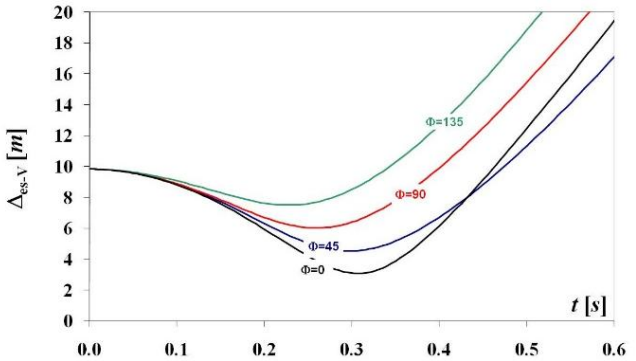

Fig. 25. Distance between the seat and the stabilizer. Source: own work

References

1. Bastug, E., Serin, N., Elaldi, F. (2025). Trajectory analysis and flight modeling of combat aircrafts ejection seats. *Chinese Journal of Aeronautics*, 38(2), 103267, https://doi.org/10.1016/j.cja.2024.09.043.
2. Chen, D. H., Wu, W. H., Wang J. J., Huang Y. (2007). Investigation on the aerodynamic performance of an ejection seat. *The Aeronautical Journal*, 111(1120), 373-380, https://doi.org/10.1017/S0001924000004620.
3. Dowództwo Wojsk Lotniczych (1985). Fotel katapultowy K-36DM. Opis techniczny i eksploatacja.
4. Głowiński, S., Krzyżyński, T. (2010). Simulation of trajectory of an aircraft seat ejection. *Symulacja w Badaniach i Rozwoju*, 1, 4, 343-351.
5. Głowiński, S., Krzyżyński, T. (2011). On modeling of ejection process in a training combat aircraft. *Archives of Transport*, 23(3), 291-302, https://doi.org/10.2478/v10174-011-0020-y.
6. Głowiński, S., Krzyżyński, T. (2013). Modelling of the Ejection Process in a Symmetrical Flight. *Journal of Theoretical and Applied Mechanics*, 51, 3, 775-785.
7. Gołda, P., Zawisza, T., & Izdebski, M. (2021). Evaluation of efficiency and reliability of airport processes using simulation tools. *Eksploatacja i Niezawodność*, *23*(4): 659-669, https://doi.org/10.17531/ein.2021.4.8.
8. Izdebski, M., Jacyna, M., Bogdański, J. (2024). Minimisation of the Energy Expenditure of Electric Vehicles in Municipal Service Companies, Taking into Account the Uncertainty of Charging Point Operation, *Energies*, t.17, s. 1–21, https://doi.org/10.3390/en17092179.
9. Izdebski, M., Jacyna-Gołda, I., Gołębiowski, P., & Plandor, J. (2020). The optmization tool supporting supply chain management in the multi-criteria approach. *Archives of Civil Engineering*, 66(3), 505-524, https://doi.org/10.24425/ace.2020.134410.
10. Izdebski, M., Michalska, A., Jacyna-Gołda, I., Gherman, L. (2024). Prediction of cyber-attacks in air transport using neural networks. *Eksploatacja i Niezawodnosc – Maintenance and Reliability*, 26(4), 191476, http://doi.org/10.17531/ein/191476.
11. Jacyna, M., Żochowska, R., Sobota, A., & Wasiak, M. (2022). Decision support for choosing a scenario for organizing urban transport system with share of electric vehicles. *Zeszyty Naukowe. Transport/Politechnika Śląska,* 117, 69-89, https://doi.org/10.20858/sjsutst.2022.117.5.
12. Jacyna-Gołda, I., Izdebski, M., & Murawski, J. (2017). The assumptions to the ant algorithm in the assignment of vehicles to tasks in the production companies. In *21th International Conference Transport Means*. Kaunas University of Technology, 985-991.
13. Jacyna-Gołda, I., Lewczuk, K., Szczepański, E., & Murawski, J. (2015). Computer Aided Implementation of Logistics Processes–Selected Aspects. *In International Conference on Transport Systems*

Telematics. Cham: Springer International Publishing, 67-80, https://doi.org/10.1007/978-3-319-24577-5_7.
14. Kowaleczko, G., Długołęcki, A., Sosnowski M. (2018). The mathematical model of the pilot's ejection proces by using the K-36DM ejection seat. *Journal of KONBiN*, 48, 515 - 528, https://doi.org/10.2478/jok-2018-0069.
15. Kowalski, M., Izdebski, M., Żak, J., Gołda, P., & Manerowski, J. (2021). Planning and management of aircraft maintenance using a genetic algorithm. *Eksploatacja i Niezawodność*, 23(1):143-153, https://doi.org/10.17531/ein.2021.1.15.
16. Lasota, M. K., Sokołowski, M., Wojdat, C., & Pierzak, A. (2025). Risk of adverse events in the transportation of oversize cargoes. *Maintenance & Reliability/Eksploatacja i Niezawodność*, *27*(1): 197383, https://doi.org/10.17531/ein/197383.
17. Lasota, M., Jacyna, M., & Szaciłło, L. (2024). Fault tree method as a decision-making tool for assessing the risks of transportation of dangerous loads. *Zeszyty Naukowe. Transport/Politechnika Śląska*, 123, 133-154, https://doi.org/10.20858/sjsutst.2024.123.6.
18. Mao, XD, Lin, GP, Yu, J. (2011). Predicting ejection velocity of ejection seat via back propagation neural network. *J Aircr*, 48(2):668, https://doi.org/10.2514/1.C031196.
19. Maryniak, J., Maryniak, A., Ładyżyńska-Kozdraś, E., Folte, U. (2004). Modelowanie i symulacja numeryczna katapultowania z samolotu systemu fotel+pilot – obciążenie pilota. *Mechanika w Lotnictwie*, XI.
20. Naveen, Raj, R., Shankar, K. (2022). A two stage neural network for choosing optimal ejection parameters in low altitude seat ejection based on novel injury parameter. *Optim Eng* 23, 827–853, https://doi.org/10.1007/s11081-021-09607-1.
21. Parate, B. A. (2022). Science And Technology of Aircraft Seat Ejection: Advanced Concepts. *Cogent Engineering*, 9(1): 2034267, https://doi.org/10.1080/23311916.2022.2034267.
22. Rahman, M.M., Prakash, V., Chandel1 S., Thakur, D.G., Čep, R., Khedkar, N., Salunkhe, S., Abouel, Nasr E.S. (2023). Analysis of the aerodynamic characteristics of an ejection seat system using computational fluid dynamics, *Frontiers in Mechanical Engineering*, 9:1255051, https://doi: 10.3389/fmech.2023.1255051.
23. Ramm, A.G., Kaleps, I. (1994). Modeling of the ejection process. Mathematical and Computer Modelling, 20(1), 95-101, https://doi.org/10.1016/0895-7177(94)90221-6.
24. Reichenau, D.E.A. (1972). Aerodynamic Characteristics of an Ejection Seat Escape System with a Stabilization Parachute at Mach Numbers from 0.3 throught 1.2, *AEDC-TR-72-51*, 42.
25. Semenov, I., Jacyna, M., Auguściak, I., & Wasiak, M. (2025). Hybrid Human–AI Collaboration for Optimized Fuel Delivery Management. *Energies*, *18*(19), 5203. https://doi.org/10.3390/en18195203.
26. Stępień, S, Szajnar, S, Jasztal, M. (2017). Problems of military aircraft crew's safety in condition of enemy counteraction. Eksploatacja i Niezawodnosc – Maintenance and Reliability, 19(3), 441–446, http://dx.doi.org/10.17531/ein.2017.3.15.
27. Szajnar, S., Jasztal, M. (2002). Wyznaczenie i analiza charakterystyk masowych układu fotel katapultowy – pilot, *Biuletyn WAT*, Vol. 51, nr 8, 59-71.
28. Szczepański, E., Jacyna-Gołda, I., & Murawski, J. (2014). Genetic algorithms based approach for transhipment hub location in urban areas. *Archives of Transport*, 31(3), 73-82, https://doi.org/10.5604/08669546.1146989.
29. Szczepański, E., Żak, J., Jacyna-Gołda, I., & Murawski, J. (2017). Simulation support of freight delivery schedule in urban areas. *Procedia Engineering*, *187*, 520-525.
30. Szendzielorz, Cz. (1986). Dynamika ruchu fotela odrzucanego względem samolotu w locie symetrycznym, *Mechanika Teoretyczna i Stosowana*, 1/2, 24.
31. Voleti, S., McLean, A. L., Upchurch, E. H., Hampton, J. L., Sugiyama, H., & Richard, H. A. (2024). A Multi-domain Simulation Framework for Modeling an Aircraft Ejection Event. In *AIAA SCITECH 2024 Forum*, https://doi.org/10.2514/6.2024-0049.

32. Wachnik, B., Pryciński, P., Murawski, J., & Nader, M. (2021). An analysis of the causes and consequences of the information gap in IT projects. The client's and the supplier's perspective in Poland. *Archives of Transport*, 60(4), 219-244, https://doi.org/ 10.1117/12.3064981.
33. Yu, J., Lin, G., Mao, X. (2010). Numerical Simulation of Ejection Seat and Analysis of Performance Under Adverse Attitudes. *Acta Aeronautica et Astronautica Sinica*, 31(10): 1927-1932.
34. Zhang, D. (2009). The Numerical Simulation of Flow Around Ejection System, *Modern Physics Letters B*, 23, 3, 489-492, https://doi.org/10.1142/S0217984909018722.